Materials Horizons

ROYAL SOCIETY OF CHEMISTRY

COMMUNICATION

View Article Online
View Journal | View Issue

Cite this: *Mater. Horiz.*, 2023, 10, 4224

Received 8th June 2023,
Accepted 27th July 2023

DOI: 10.1039/d3mh00881a

rsc.li/materials-horizons

Integrating the atomically separated frontier molecular orbital distribution of two multiple resonance frameworks through a single bond for high-efficiency narrowband emission†

Meng-Yuan Chen,‡[a] Feng Huang,‡[a] Hao Wu,[a] Ying-Chun Cheng,[a] Hui Wang,[a] Ya-Nan Hu,[a] Xiao-Chun Fan,[a] Jia Yu,[ab] Kai Wang *[ac] and Xiao-Hong Zhang *[ab]

Atomically separated frontier molecular orbital (FMO) distribution plays a crucial role in achieving narrowband emissions for multiple resonance (MR)-type thermally activated delayed fluorescence emitters. Directly peripherally decorating a MR framework with donor or acceptor groups is a common strategy for developing MR emitters. However, this approach always induces bonding features and thus spectral broadening as a side effect. How direct donor/acceptor decoration enhances atomic FMO separation while avoiding bonding features has not been explored. For this aim, two MR derivatives are synthesized by integrating two MR frameworks at different sites. Following resonance alignment, DOBNA-*m*-CzBN avoids breaking nonbonding FMO features at the single connecting bond and shows enhanced MR characteristics, with a sharp emission at 491 nm and a full width at half maximum (FWHM) of 24 nm/118 meV. Conversely, DOBNA-*p*-CzBN emerges as a bonding feature due to its continuous π-conjugation extension, with a broadened FWHM of 26 nm/132 meV peaking at 497 nm. Impressively, both emitters exhibit outstanding external quantum efficiencies of 37.8–38.6% in organic light-emitting diodes (OLEDs), demonstrating improved performance with rigid acceptor decoration. Distinctly, the electroluminescence of DOBNA-*m*-CzBN shows a narrower FWHM than that of DOBNA-*p*-CzBN. This work for the first time reports the enhancement of atomic FMO separation for MR emitters *via* peripheral decoration through a single bond and provides a more comprehensive illustration for further development of MR emitters.

[a] *Institute of Functional Nano & Soft Materials (FUNSOM), Soochow University, Suzhou, Jiangsu 215123, P. R. China. E-mail: wkai@suda.edu.cn, xiaohong_zhang@suda.edu.cn*

[b] *Jiangsu Key Laboratory of Advanced Negative Carbon Technologies, Soochow University, Suzhou, Jiangsu 215123, P. R. China*

[c] *Jiangsu Key Laboratory for Carbon-Based Functional Materials & Devices, Soochow University, Suzhou, Jiangsu, 215123, P. R. China*

† Electronic supplementary information (ESI) available. See DOI: https://doi.org/10.1039/d3mh00881a

‡ These authors contributed equally to the work.

New concepts

Colour purity is an important parameter for organic light-emitting diodes (OLEDs) for their display applications. Compounds with multiple resonance (MR) features are promising OLED emitters for achieving high colour purity and high efficiency electroluminescence. Their unique atomic frontier molecular orbital (FMO) separation is critical to minimizing vibronic coupling and vibrational relaxation, and thus beneficial for reducing the emission bandwidth. A commonly applied design strategy for new MR compounds is direct peripheral decoration on an original MR framework; however, it always introduces unexpected bonding features and spectral broadening. Until now, how atomic FMO separation has been enhanced through a single bond has remained confusing and challenging. To explore this problem, two isomers were developed by integrating two MR frameworks through a single bond at different linking positions. According to their different photophysical properties and device performances, we conclude that enhanced atomic FMO separation can be realized when linking to the position following resonance alignment, giving rise to a narrower emission bandwidth. Conversely, bonding features will be introduced when linking to the position with continuous π-conjugation, which broadens its spectral bandwidth. This work for the first time reports the enhancement of atomic FMO separation for MR emitters *via* peripheral decoration through a single bond, providing a more comprehensive illustration for further development of MR emitters.

Introduction

Thermally activated delayed fluorescence (TADF) materials have become popular as emitters for organic light-emitting diodes (OLEDs) due to their potential to achieve 100% internal quantum efficiencies (IQEs).[1–6] Highly twisted electron donor–acceptor (D–A) molecular geometries are the most commonly noticed forms for TADF emitters, showing separated front molecular orbitals (FMOs), which are a prerequisite for reducing the energy gaps (ΔE_{ST}s) between the lowest singlet (S_1) and triplet (T_1) excited states and promoting the reverse intersystem crossing (RISC) process (*i.e.*, $T_1 \rightarrow S_1$).[7–23] However, D–A-type TADF emitters generally suffer from serious structural relaxations upon excitation, giving rise to large Stokes shifts and broadband emissions with full width at half maxima (FWHM) typically beyond 70 nm, which are detrimental to their application toward ultrahigh definition (UHD) displays.[24–29]

In 2016, Hatakeyama *et al.* pioneered a novel molecular design to achieve narrowband TADF emitters based on the multiple resonance (MR) effect.[30] The very first MR paradigm DABNA involved precise displacements of electron-donating nitrogen (N) atoms and an electron-withdrawing boron (B) atom at the *para*-position to each other within a polycyclic aromatic hydrocarbon (PAH) framework. Interestingly, the highest occupied molecular orbital (HOMO) and the lowest unoccupied molecular orbital (LUMO) of the MR framework appear to have unique atomically separated distributions, also giving rise to an unexpected small molecular ΔE_{ST}. More importantly, with such a highly robust framework, its molecular relaxation can be well suppressed. Thus, the compounds not only succeed in gaining TADF properties but also exhibit small Stokes shifts and narrowband emissions. In 2019, the same group further developed a double boron-embedded MR emitter, ν-DABNA, with similar B/N distributions to DABNA but with a more extended π-conjugation.[31] ν-DABNA shows an even more obvious atomic HOMO–LUMO separation due to a stronger MR effect caused by more heteroatoms. As a result, a ν-DABNA-based OLED exhibited an extremely sharp blue emission with an FWHM of 18 nm/81 meV (*ca.*) and an impressive maximum external quantum efficiency (EQE_{max}) of 34.4%. Importantly, in that work, they further pointed out that such unique FMO distributions with obvious nonbonding features also play an important role in minimizing vibronic coupling and vibrational relaxation. This viewpoint has been repeatedly verified in several subsequent studies.[32,33] These results provide a promising direction towards realizing ultranarrow band emissions of organic emitters, *i.e.*, to construct large fused MR frameworks integrating more doped B/N atoms with stronger atomic FMO distributions. Recently, Kido *et al.* designed three MR emitters, which are PAHs with embedded B/N and oxygen (O) atoms, demonstrating that larger fused MR frameworks with more doped B/N/O atoms can also exhibit higher colour purity.[34] However, great challenges remain for such MR frameworks with a large extended π-conjugation in terms of issues such as chemical synthesis (*e.g.*, multiple byproducts and purification difficulties) and derivations.[35–41] In contrast, another important direction for designing MR emitters is peripheral decoration on an MR framework directly through a single bond, which may offer a more accessible method for functionalization for different demands.[42–51] For example, in 2020, Wang *et al.* reported a green MR-TADF emitter, *m*-Cz-BNCz, in which an additional electron-donating carbazole unit was introduced onto the *meta*-position of the boron atom of DtBuCzB, a classical MR framework.[33] The compound showed a sharp emission at 519 nm in toluene solution and a high EQE of 31.4% in OLEDs. However, spectral broadening was also observed for *m*-Cz-BNCz with an increased FWHM of 43 nm/171 meV (*ca.*) in devices compared to the MR framework. Similar results are often noticed among MR framework derivatives with simple peripheral decoration, *i.e.*, improved efficiency with reduced colour purity as a side effect.[7,52] This is because introducing such decorations breaks the precise atomical FMO separation of MR frameworks at the single connecting bonds, bringing about long-range charge-transfer (CT) features to the overall compounds, which is highly related to molecular relaxations and spectral broadening. To date, it is still an open question whether the nonbonding features of MR frameworks could be enhanced rather than weakened *via* direct peripheral decoration.

Here, we proposed a novel MR decoration strategy, *i.e.*, connecting two MR featured frameworks with precisely modulated connecting sites, to avoid breaking nonbonding FMO features at the single connecting bond and even achieve an enhanced nonbonding FMO feature. A proof-of-concept emitter (DOBNA-*m*-CzBN) and a control compound (DOBNA-*p*-CzBN) were thus developed by attaching 5,9-dioxa-13b-boranaphtho[3,2,1-*de*]anthracene (DOBNA) onto DtBuCzB (whose main body is CzBN) at the *meta*- and *para*-sites to the boron atom, respectively (see Fig. 1). In contrast to the common peripheral decoration without MR properties, which may bring about long-range CT contribution and are detrimental to the colour purity,[52,53] our employed decoration unit (DOBNA) is a typical MR framework with an overall electron-deficient character. Specifically, for DOBNA-*m*-CzBN, the decoration is linked to a HOMO-occupied carbon atom following resonance alignment, thereby enhancing its atomic FMO separation, which further reduces its emission bandwidth. This is distinctly different from that of the control compound, in which the decoration is linked to a LUMO-occupied carbon atom disturbing the MR featured distribution inside its core and brings formal bonding features. Thus, DOBNA-*p*-CzBN with continuous π-conjugation introduces a long-range CT component that harms its bandwidth and colour purity. In contrast, DOBNA-*m*-CzBN exhibits a reduced emission bandwidth due to its stronger MR effect. In toluene solution, DOBNA-*m*-CzBN gives an evidently narrower emission with an FWHM of 24 nm/118 meV than DOBNA-*p*-CzBN (26 nm/132 meV). This result is even narrower than the original MR framework CzBN (23 nm/129 meV) in energy units, demonstrating its enhanced MR characteristics. In OLEDs, both emitters present similar exceptional EQE_{max} values of 37.8–38.6%. Our work for the first time provides a solution for the

Kai Wang

Over the past decade, Materials Horizons has emerged as one of the leading journals in the field of materials sciences. I take great pride in the fact that four of our papers have been published in this outstanding journal. Being chosen as an Emerging Investigator Series author of Materials Horizons in 2022 is a tremendous honor for me. I would like to extend my heartfelt congratulations on the journal's 10th anniversary and send my best wishes for its continued success. I hope that in the next decade, we can contribute even more exciting and groundbreaking research to Materials Horizons.

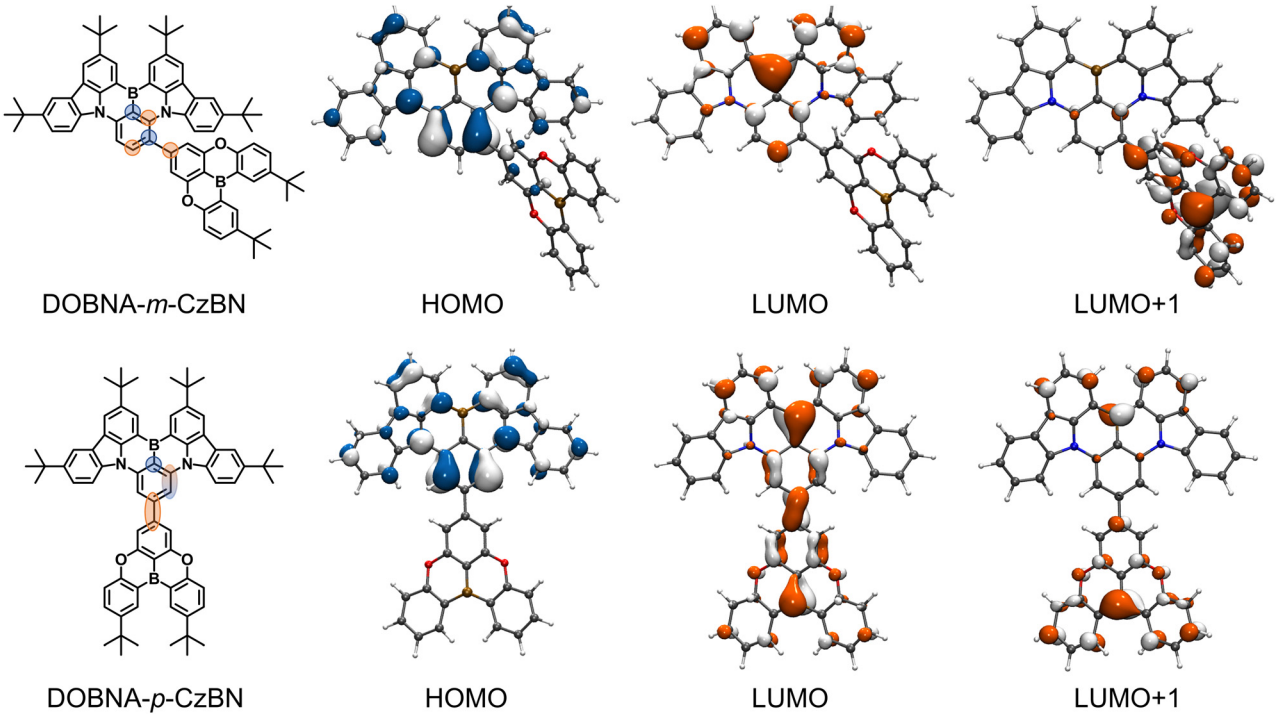

Fig. 1 The chemical structures and frontier molecular orbital (FMO) distributions of DOBNA-*m*-CzBN and DOBNA-*p*-CzBN.

enhancement of the atomic FMO separation features of MR emitters with peripheral decoration through a single bond, thus promoting the development of narrowband MR emitters with better colour purity.

Results and discussion

Synthesis and characterization

Scheme S1 (ESI†) exhibits the synthetic routes for the target compounds. The intermediates *m*-Br-BNCz, *p*-Br-BNCz and DOBNA-Bpin were first synthesized according to the reported procedures.[7,54–56] Then, the target compounds can be achieved *via* palladium-catalyzed Buchwald–Hartwig cross-coupling reactions of the intermediates. The chemical structures of the target compounds were characterized using nuclear magnetic resonance (NMR) spectroscopy and mass spectrometry. As displayed in Fig. S1 (ESI†), both DOBNA-*m*-CzBN and DOBNA-*p*-CzBN depict excellent thermal stability with high decomposition temperatures (T_d) of 465 and 508 °C, respectively. Additionally, there are no obvious glass transitions observed below 350 °C, guaranteeing their application in evaporation processes.

Theoretical calculations

To investigate the effects of DOBNA decoration on different sites of BNCz, density functional theory (DFT) calculations are performed in ground states (Fig. 1). Due to the stronger electron-donating properties of CzBN, the HOMOs of both emitters depend mainly on their CzBN components with almost identical distributions and are very mildly extended to the DOBNA parts. These distributions are clearly atomically separated due to the MR effect inside the CzBN components. On the other hand, their unoccupied FMO distributions demonstrate interesting differences. In contrast to common acceptors, the LUMO/LUMO+1 in DOBNA parts basically obey the atomic FMO separation as an MR component. Distinctly, in the case of DOBNA-*m*-CzBN, the DOBNA decoration is linked to the HOMO-occupied carbon atom, following the resonance alignment of the opposite arrangement of B/N atoms. Hence, the intrinsic atomic distribution with nonbonding features is more pronounced and observed inside the CzBN core. Nevertheless, DOBNA-*p*-CzBN favors unwanted bonding features, as the DOBNA decoration is linked to the LUMO-occupied carbon atom, which extends continuous π-conjugation. Fig. S2 (ESI†) summarizes the atomic contributions to the FMOs inside the CzBN segment, further demonstrating these different bonding/nonbonding features. This distinct difference can be further ascribed to the MR effect inside the DOBNA part. For either compound, the connecting position on the DOBNA part is the carbon atom *para*-positioned to the boron atom and *meta*-positioned to the nitrogen atoms, which is clearly an electron-density decreased site. Therefore, when linking it to the *meta*-position of the boron atom (*i.e.*, DOBNA-*m*-CzBN), which is an electron-density increased site, the MR effects inside the two frameworks are consistent with each other, leading to further superimposed results. However, when linking it to the *para*-position of the boron atom (*i.e.*, DOBNA-*p*-CzBN), which is an electron-density decreased site, two electron-deficient carbon atoms as the bridge would lead to continuous π-conjugations rather than atomic separations. As a result, a long-range CT

transition may occur between the DOBNA and CzBN segments. To verify this assumption, natural transition orbital (NTO) analysis is performed, as depicted in Fig. S3 (ESI†). For both compounds, while their NTO distributions show apparent differences, the S_1 and T_1 states of each compound exhibit similar NTO delocalization profiles. Consequently, their spin–orbit couplings (SOCs) between the S_1 and T_1 manifolds are both negligible (*ca.* 0.04 cm^{-1}). For DOBNA-*m*-CzBN, the hole and particle distributions are both almost located on the CzBN framework, obeying an MR-dominated feature. For DOBNA-*p*-CzBN, the holes remain on the CzBN frameworks as well, while the particles expand to the entire molecule. Such NTO distributions lead to both its S_1 and T_1 states with mixed features that combine characteristics of long-range CT and MR. Furthermore, by comparing the geometries of their ground and S_1 states, the root-mean-square deviations (RMSDs) are calculated as 0.098 and 0.242 Å for DOBNA-*m*-CzBN and DOBNA-*p*-CzBN, respectively. The lower RMSD value of DOBNA-*m*-CzBN further confirms its well-maintained MR features (Fig. S4, ESI†).

Electrochemical properties

Fig. S5 (ESI†) illustrates the oxidation curves of both compounds using cyclic voltammetry (CV) measurements. Based on the oxidation onsets, the HOMO energy levels are estimated to be −5.40 eV for DOBNA-*m*-CzBN and −5.46 eV for DOBNA-*p*-CzBN. By using the HOMO energy levels and their optical bandgaps (*vide infra*), their LUMO energy levels are further determined to be −2.88 and −2.97 eV, respectively.

Photophysical properties

To explore their photophysical properties, the UV-Vis absorption and PL spectra of both emitters were measured in toluene solution (1.0×10^{-5} M) at room temperature (Fig. 2). Conspicuous MR-featured absorption and emission bands are observed with peaks at 474 and 491 nm for DOBNA-*m*-CzBN and 477 and 497 nm for DOBNA-*p*-CzBN, respectively, giving rise to small Stokes shifts of 17 and 20 nm. These very similar photophysical properties are reasonable, as they consist of identical components. However, it is worth noting that another important parameter of MR compounds, *i.e.*, their emission bandwidths, shows noticeable differences. The emissive FWHM of DOBNA-*m*-CzBN is only 24 nm/118 meV, which is not only evidently narrower than that of DOBNA-*p*-CzBN (26 nm/132 meV) but even slightly smaller than that of the original CzBN molecule (24 nm/129 meV), indicating its obviously enhanced nonbonding feature. This FWHM difference is even more obvious when comparing their emission spectra when doped in 9-(2-(9-phenyl-9*H*carbazol-3-yl)phenyl)-9*H*-3,9′-bicarbazole (PhCzBCz) at a 3 wt% concentration. As shown in Fig. 2 and Table 1, at room temperature, the DOBNA-*m*-CzBN-based film shows a narrowband emission peaking at 496 nm with a spectral FWHM of 130 meV (25 nm), similar to that in toluene, while the emission of the DOBNA-*p*-CzBN-based film is redshifted to 506 nm, and the FWHM even extends to 161 meV (34 nm). The different environmental sensitivity behaviours of the isomers should be mainly ascribed to their different molecular polarities. We then used solvation effect measurements to further evaluate their dipole moments (Fig. S6 and S7, details seen in Table S1 and S2, ESI†). At various solvents, both emitters always display monopeaks with slight spectral shifts. Such phenomena are distinctly different from the recent report by Yang *et al.*, where a typical donor 10H-phenoxazine is taken to decorate onto the same MR framework (CzBN), showing an obvious solvation effect and double-peaked emissions especially in high-polarity solvents due to the contribution of strong long-range CT and varied energy level alignments.[57] As shown in Fig. S8 (ESI†), DOBNA-*m*-CzBN is determined to have a smaller dipole moment of 0.98 D compared to DOBNA-*p*-CzBN (1.47 D). Thus, it is reasonable that DOBNA-*m*-CzBN with more obvious nonbonding features could achieve a relatively stable narrowband emission under different conditions.

Their fluorescence and phosphorescence spectra are further measured in toluene at 77 K (Fig. 2), and the S_1/T_1 energy levels are thus estimated to be 2.62/2.48 and 2.58/2.45 eV for

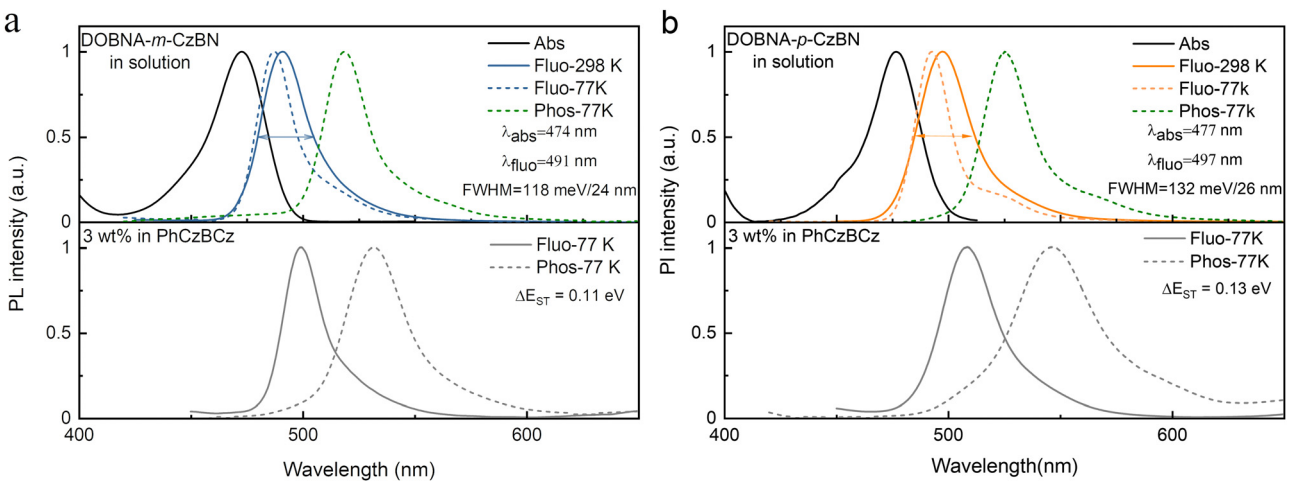

Fig. 2 UV–vis absorption and photoluminescence spectra of (a) DOBNA-*m*-CzBN and (b) DOBNA-*p*-CzBN in diluted toluene (upper) and in PhCzBCz films (below).

DOBNA-*m*-CzBN and DOBNA-*p*-CzBN, respectively, affording similar ΔE_{ST} values of 0.14 and 0.13 eV, respectively, which are small enough for realizing TADF. Notably compared to their fluorescence spectra in toluene, the fluorescence spectra of the DOBNA-*m*-CzBN- and DOBNA-*p*-CzBN-based films exhibit redshifts of approximately 12 and 17 nm, respectively. This bathochromic shift can be attributed to solid solvent effects. The surrounding environment in PhCzBCz films differs from that in the solvent, affecting the charge distribution and interaction mode of the emitters. Generally, the PhCzBCz film exhibits a higher polarity compared to the toluene solvent, which results in a spectral redshift.[52] Meanwhile, we also noticed mild shoulders in the PL spectra of the films at 77 K. This might be the influence of their phosphorescence due to the suppressed triplet nonradiative decays. At room temperature, the RISC and nonradiative decays of triplet excitons are both accelerated, resulting in the absence of the shoulders and Gaussian distribution profiles.

Transient PL decay curves of 3 wt% DOBNA-*m*-CzBN and DOBNA-*p*-CzBN doped in PhCzBCz films are measured at room temperature to confirm their TADF properties. Fig. S9 (ESI†) shows prompt and delayed signals measured with 100 ns and 200 μs time windows, respectively. The clear fluorescence intensities lasting dozens of microseconds confirm their TADF features. Such delayed lifetimes are similar to the original MR CzBN.[42] The relatively large ΔE_{ST}s and small SOC values should be the main reason for the slow upconversion of triplets and long lifetimes. By using an integrating sphere measurement under a nitrogen atmosphere upon excitation at 300 nm, the PLQYs of both the DOBNA-*m*-CzBN and DOBNA-*p*-CzBN films are measured to have similar values of 95.1% and 96.2%, respectively. Based on the PLQYs, lifetimes, and contributions of prompt and delayed fluorescence, the key kinetic parameters are calculated and summarized in Table S3 (ESI†). DOBNA-*m*-CzBN shows a slightly faster singlet radiation decay rate (k_r^S) of 7.2×10^7 s^{-1} compared to DOBNA-*p*-CzBN (k_r^S of 5.0×10^7 s^{-1}), agreeing with its larger oscillator strength. On the other hand, both compounds display similar RISC rates (k_{RISC}s) enough to surpass the triplet nonradiative decay rates (k_{nr}^Ts), thus leading to a sufficient RISC process for triplet excitons.

Furthermore, with the expectation that the planarity of the CzBN and DOBNA framework may contribute to molecular horizontal orientations, we carried out angle-dependent PL measurements on their doped films. As shown in Fig. S10 (ESI†), both isomers in the diluted films exhibit clearly preferred horizontal emitting dipole orientations with impressive horizontal ratios of 92% and 93% for DOBNA-*m*-CzBN and DOBNA-*p*-CzBN, respectively. These results would greatly enhance the light out-coupling efficiency and eventually help to enhance their performance in devices.

Device performance

To further evaluate their electroluminescence (EL) properties, OLEDs are fabricated with the following optimized device structure: ITO (indium tin oxide)/TAPC (4,4′-cyclohexylidenebis[*N*,*N*-bis(*p*-tolyl)aniline]) (30 nm)/TCTA (4,4′,4″-tris(carbazol-9-yi)triphenylamine) (10 nm)/emitting layer (20 nm)/TmPyPB (1,3,5-tri[(3-pyridyl)-phen-3-yl]benzene) (40 nm)/LiF (1 nm)/Al, as shown in Fig. 3(a). In the device, ITO and Al act as the anode and cathode, respectively; TAPC and TCTA are selected as the hole transporting and electron blocking layers, respectively; TmPyPB and LiF serve as the electron transporting and injection layers, respectively; and PhCzBCz is selected as the host due to its high T_1 energy level, which is enough to sensitize the emitters. The optimized doping ratio is 3 wt%, and the optimization details are shown in Table S4 and S5 (ESI†). As shown in Fig. 3(c) and (d) and summarized in Table 2, both optimized devices achieved similar outstanding EQE_{max}s of 38.6% for DOBNA-*m*-CzBN and 37.8% for DOBNA-*p*-CzBN, and trends with increasing luminance. These efficiency behaviors are much superior to those of the reported devices based on the original CzBN emitter, revealing the importance of extending π-conjugations of MR emitters. These results agree well with their similar high PLQYs and splendid horizontal emitting dipole orientations. However, it should be noted that due to the relatively low k_{RISC}s, severe triplet accumulation occurred for both devices at high luminance, resulting in dramatic efficiency drop-offs *via* exciton quenching processes (*e.g.*, triplet–triplet annihilation). On the other hand, their EL spectra depict considerable differences. As shown in Fig. 3(b), the DOBNA-*m*-CzBN-based device exhibits a sharp emission band at 497 nm with an FWHM of only 28 nm/141 meV, which is not only bluer than that of the DOBNA-*p*-CzBN-based device (511 nm) but also, more importantly, evidently narrower in terms of the EL bandwidth (38 nm/177 meV). These results are consistent with their PL behaviours under identical environmental conditions, confirming the contribution of nonbonding π-extension features *via* the precisely modulated decoration strategy. With increasing luminance, the variations in

Table 1 Summary of the photophysical properties of the emitters

	3wt% in PhCzBCz@77 K				In toluene@r.t.			In toluene@77 K		
Emitters	λ_{Fl}[a] [nm]	λ_{Pho}[a] [nm]	ΔE_{ST}[b] [eV]	FWHM[c] [nm]/[meV]	λ_{Abs}[d] [nm]	λ_{Fl}[d] [nm]	FWHM[e] [nm]/[meV]	λ_{Fl}[f] [nm]	λ_{Pho}[f] [nm]	ΔE_{ST}[g] [eV]
DOBNA-*m*-CzBN	499	532	0.11	25/130	474	491	24/118	487	519	0.14
DOBNA-*P*-CzBN	509	546	0.13	34/161	477	497	26/132	492	525	0.13

[a] Estimated from the peak of the fluorescence and phosphorescence spectra of emitters doped in films at 77 K. [b] Determined from the films at 77 K. [c] FWHMs of the photoluminescence spectra in the films. [d] Estimated from the maxima of absorption and emission spectra in dilute toluene solution at room temperature. [e] FWHMs of the photoluminescence spectra in dilute toluene solution at room temperature. [f] Estimated from the peak of the fluorescence and phosphorescence spectra in dilute toluene solution at 77 K. [g] Determined in dilute toluene solution at 77 K.

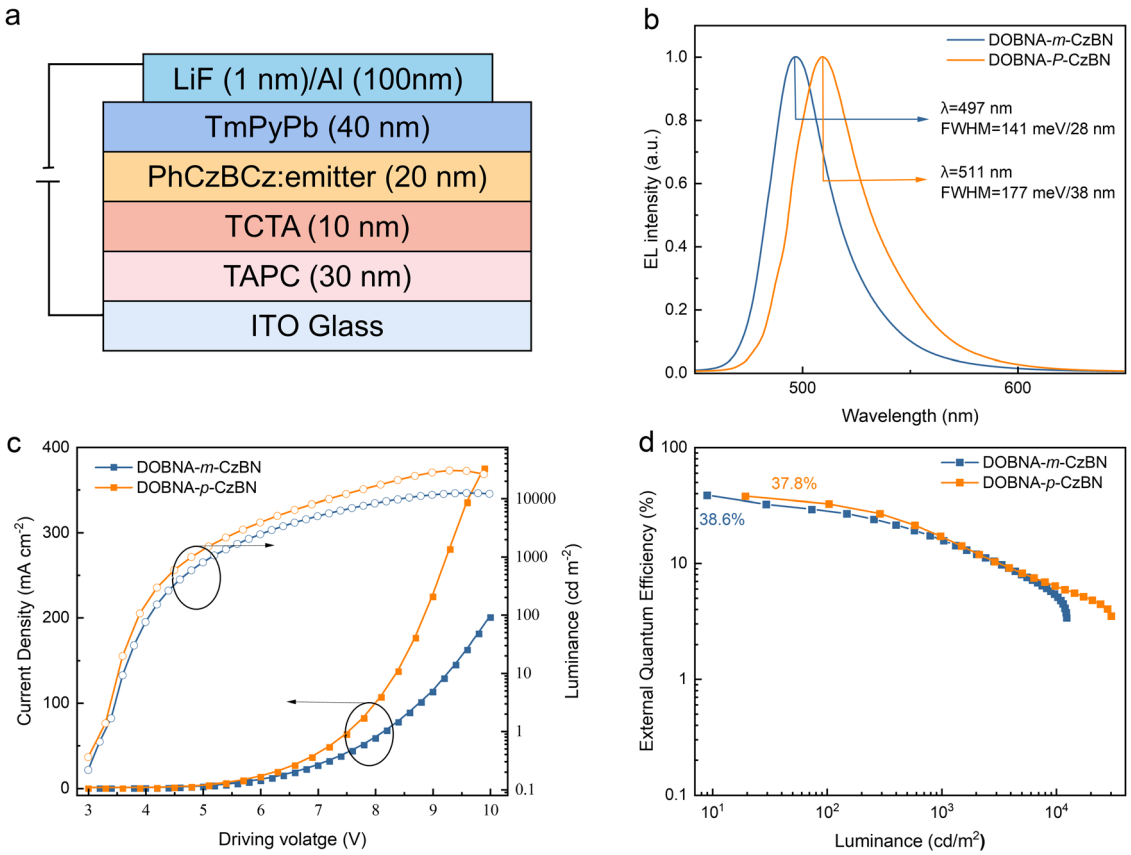

Fig. 3 Device structure and performance of OLEDs. (a) Device configuration. (b) Normalized electroluminescence spectrum. (c) Current density–voltage–luminance curves. (d) EQE–luminance curves.

Table 2 EL performances of OLEDs based on DOBNA-*m*-CzBN and DOBNA-*p* CzBN emitters

Emitters	λ_{em}[a] [nm]	FWHM[b] [nm]/[meV]	PE_{max}[c] [lm W^{-1}]	CE_{max}[d] [cd A^{-1}]	$EQE_{max/1000}$[e] [%]	CIE[f] (x, y)
DOBNA-*m*-CzBN	497	28/141	84.6	91.5	38.6/15.7	(0.11, 0.54)
DOBNA-*p*-CzBN	511	38/177	105.2	120.5	37.8/17.2	(0.17, 0.67)

[a] Peak wavelength of the EL spectra. [b] Full width at half-maximum. [c] Maximum power efficiency. [d] Maximum current efficiency. [e] Maximum external quantum efficiency, and values at 1000 cd m^{-2}. [f] Recorded at 1000 cd m^{-2}.

the EL spectra are negligible, as shown in Fig. S11 (ESI†), demonstrating its good spectral stability.

Conclusions

In summary, two MR derivatives, DOBNA-*m*-CzBN and DOBNA-*p*-CzBN, are synthesized with an MR-featured DOBNA decoration of distinct binding sites to an MR framework CzBN. Following resonance alignment, DOBNA-*m*-CzBN is found to have an even enhanced atomic FMO separation. In contrast, the bonding feature is introduced into DOBNA-*p*-CzBN for its continuous π-conjugation extension. As a result, DOBNA-*m*-CzBN exhibits a sharper emission with a peak at 491 nm and an FWHM of 24 nm/118 meV compared to that of DOBNA-*p*-CzBN (a peak at 497 nm and an FWHM of 26 nm/132 meV). The rigidity of the decoration improves their PLQYs and horizontal dipole orientations. Therefore, OLEDs employing these emitters achieve both superior EQE_{max}s of 37.8–38.6% due to their high PLQYs and efficient k_{RISC}s. Distinctly, the DOBNA-*m*-CzBN-based device shows a much more intrinsic MR-featured emission with an FWHM of 28 nm/141 meV peaking at 497 nm compared with the DOBNA-*p*-CzBN-based device, whose emission shows a spectral bathochromic peaking at 511 nm and broadening to 38 nm/177 meV. This work first realizes the enhancement of atomically separated FMO for MR emitters *via* direct peripheral acceptor decoration, paving a way for further development of narrowband MR emitters.

Conflicts of interest

There are no conflicts to declare.

Acknowledgements

This work was supported by the National Natural Science Foundation of China (Grant No. 52130304, 51821002, and 52003185), the National Key Research & Development Program of China (Grant No. 2020YFA0714601, 2020YFA0714604), the Science and Technology Program of Suzhou (Grant No. ZXL2022490), Suzhou Key Laboratory of Functional Nano & Soft Materials, Collaborative Innovation Center of Suzhou Nano Science & Technology, and the 111 Project, Joint International Research Laboratory of Carbon-Based Functional Materials and Devices.

References

1 Y. Tao, K. Yuan, T. Chen, P. Xu, H. H. Li, R. F. Chen, C. Zheng, L. Zhang and W. Huang, *Adv. Mater.*, 2014, **26**, 7931–7958.
2 S. Y. Lee, T. Yasuda, H. Nomura and C. Adachi, *Appl. Phys. Lett.*, 2012, **101**, 093306.
3 A. Endo, K. Sato, K. Yoshimura, T. Kai, A. Kawada, H. Miyazaki and C. Adachi, *Appl. Phys. Lett.*, 2011, **98**, 083302.
4 H. Uoyama, K. Goushi, K. Shizu, H. Nomura and C. Adachi, *Nature*, 2012, **492**, 234–238.
5 M. A. Baldo, S. Lamansky, P. E. Burrows, M. E. Thompson and S. R. Forrest, *Appl. Phys. Lett.*, 1999, **75**, 4–6.
6 M. A. Baldo, D. F. O'Brien, Y. You, A. Shoustikov, S. Sibley, M. E. Thompson and S. R. Forrest, *Nature*, 1998, **395**, 151–154.
7 Y. Liu, X. Xiao, Y. Ran, Z. Y. Bin and J. S. You, *Chem. Sci.*, 2021, **12**, 9408–9412.
8 J. A. Knoller, G. Y. Meng, X. Wang, D. Hall, A. Pershin, D. Beljonne, Y. Olivier, S. Laschat, E. Zysman-Colman and S. N. Wang, *Angew. Chem., Int. Ed.*, 2020, **59**, 3156–3160.
9 M. Nagata, H. Min, E. Watanabe, H. Fukumoto, Y. Mizuhata, N. Tokitoh, T. Agou and T. Yasuda, *Angew. Chem., Int. Ed.*, 2021, **60**, 20280–20285.
10 X. Liang, Z. P. Yan, H. B. Han, Z. G. Wu, Y. X. Zheng, H. Meng, J. L. Zuo and W. Huang, *Angew. Chem., Int. Ed.*, 2018, **57**, 11316–11320.
11 S. Nakatsuka, H. Gotoh, K. Kinoshita, N. Yasuda and T. Hatakeyama, *Angew. Chem., Int. Ed.*, 2017, **56**, 5087–5090.
12 Y. W. Zhang, D. D. Zhang, T. Y. Huang, A. J. Gillett, Y. Liu, D. P. Hu, L. S. Cui, Z. Y. Bin, G. M. Li, J. B. Wei and L. Duan, *Angew. Chem., Int. Ed.*, 2021, **60**, 20498–20503.
13 Y. W. Zhang, D. D. Zhang, J. B. Wei, X. C. Hong, Y. Lu, D. P. Hu, G. M. Li, Z. Y. Liu, Y. Chen and L. Duan, *Angew. Chem., Int. Ed.*, 2020, **59**, 17499–17503.
14 X. Qiu, G. J. Tian, C. W. Lin, Y. Y. Pan, X. Y. Ye, B. H. Wang, D. G. Ma, D. H. Hu, Y. Luo and Y. G. Ma, *Adv. Opt. Mater.*, 2021, **9**, 2001845.
15 Y. F. Zhang and S. R. Forrest, *Phys. Rev. Lett.*, 2012, **108**, 267404.
16 Y. Im, M. Kim, Y. J. Cho, J. A. Seo, K. S. Yook and J. Y. Lee, *Chem. Mater.*, 2017, **29**, 1946–1963.
17 H. Noda, X. K. Chen, H. Nakanotani, T. Hosokai, M. Miyajima, N. Notsuka, Y. Kashima, J. L. Bredas and C. Adachi, *Nat. Mater.*, 2019, **18**, 1084–1090.
18 K. Suzuki, S. Kubo, K. Shizu, T. Fukushima, A. Wakamiya, Y. Murata, C. Adachi and H. Kaji, *Angew. Chem., Int. Ed.*, 2015, **54**, 15231–15235.
19 F. B. Dias, K. N. Bourdakos, V. Jankus, K. C. Moss, K. T. Kamtekar, V. Bhalla, J. Santos, M. R. Bryce and A. P. Monkman, *Adv. Mater.*, 2013, **25**, 3707–3714.
20 H. Nakanotani, Y. Tsuchiya and C. Adachi, *Chem. Lett.*, 2021, **50**, 938–948.
21 X. Y. Cai and S. J. Su, *Adv. Funct. Mater.*, 2018, **28**, 1802558.
22 J. Lee, N. Aizawa and T. Yasuda, *Chem. Mater.*, 2017, **29**, 8012–8020.
23 M. Y. Wong and E. Zysman-Colman, *Adv. Mater.*, 2017, **29**, 1605444.
24 S. Y. Lee, T. Yasuda, Y. S. Yang, Q. S. Zhang and C. Adachi, *Angew. Chem., Int. Ed.*, 2014, **53**, 6402–6406.
25 J. X. Chen, K. Wang, C. J. Zheng, M. Zhang, Y. Z. Shi, S. L. Tao, H. Lin, W. Liu, W. W. Tao, X. M. Ou and X. H. Zhang, *Adv. Sci.*, 2018, **5**, 1800436.
26 G. Z. Xie, X. L. Li, D. J. Chen, Z. H. Wang, X. Y. Cai, D. C. Chen, Y. C. Li, K. K. Liu, Y. Cao and S. J. Su, *Adv. Mater.*, 2016, **28**, 181–187.
27 S. M. Suresh, D. Hall, D. Beljonne, Y. Olivier and E. Zysman-Colman, *Adv. Funct. Mater.*, 2020, **30**, 1908677.
28 I. S. Park, K. Matsuo, N. Aizawa and T. Yasuda, *Adv. Funct. Mater.*, 2018, **28**, 1802031.
29 J. M. Teng, Y. F. Wang and C. F. Chen, *J. Mater. Chem.*, 2020, **8**, 11340–11353.
30 T. Hatakeyama, K. Shiren, K. Nakajima, S. Nomura, S. Nakatsuka, K. Kinoshita, J. P. Ni, Y. Ono and T. Ikuta, *Adv. Mater.*, 2016, **28**, 2777–2781.
31 Y. Kondo, K. Yoshiura, S. Kitera, H. Nishi, S. Oda, H. Gotoh, Y. Sasada, M. Yanai and T. Hatakeyama, *Nat. Photonics*, 2019, **13**, 678–682.
32 M. Luo, W. Li, L. Lyu, D. L. Li, S. Y. Du, M. Y. Zhao, Z. C. Wang, J. S. Zhang, Y. Li and Z. Y. Ge, *Adv. Opt. Mater.*, 2022, **11**, 2202176.
33 Y. C. Xu, C. L. Li, Z. Q. Li, Q. Y. Wang, X. L. Cai, J. B. Wei and Y. Wang, *Angew. Chem., Int. Ed.*, 2020, **59**, 17442–17446.
34 G. T. Liu, H. Sasabe, K. Kumada, H. Arai and J. Kido, *Chem. – Eur. J.*, 2022, **28**, e202202289.
35 S. S. Kothavale and J. Y. Lee, *Adv. Opt. Mater.*, 2020, **8**, 2000922.
36 S. H. Han, J. H. Jeong, J. W. Yoo and J. Y. Lee, *J. Mater. Chem.*, 2019, **7**, 3082–3089.
37 H. Tanaka, S. Oda, G. Ricci, H. Gotoh, K. Tabata, R. Kawasumi, D. Beljonne, Y. Olivier and T. Hatakeyama, *Angew. Chem., Int. Ed.*, 2021, **60**, 17910–17914.
38 S. Oda, W. Kumano, T. Hama, R. Kawasumi, K. Yoshiura and T. Hatakeyama, *Angew. Chem., Int. Ed.*, 2021, **60**, 2882–2886.
39 N. Ikeda, S. Oda, R. Matsumoto, M. Yoshioka, D. Fukushima, K. Yoshiura, N. Yasuda and T. Hatakeyama, *Adv. Mater.*, 2020, **32**, 2004072.
40 S. Oda, B. Kawakami, R. Kawasumi, R. Okita and T. Hatakeyama, *Org. Lett.*, 2019, **21**, 9311–9314.
41 K. Matsui, S. Oda, K. Yoshiura, K. Nakajima, N. Yasuda and T. Hatakeyama, *J. Am. Chem. Soc.*, 2018, **140**, 1195–1198.

42 Y. C. Xu, Z. Cheng, Z. Q. Li, B. Y. Liang, J. X. Wang, J. B. Wei, Z. L. Zhang and Y. Wang, *Adv. Opt. Mater.*, 2020, **8**, 1902142.
43 J. Park, K. J. Kim, J. Lim, T. Kim and J. Y. Lee, *Adv. Mater.*, 2022, **34**, 2108581.
44 F. T. Liu, Z. Cheng, L. Wan, Z. J. Feng, H. Liu, H. X. Jin, L. Gao, P. Lu and W. S. Yang, *Small*, 2022, **18**, 2106462.
45 P. C. Jiang, J. S. Miao, X. S. Cao, H. Xia, K. Pan, T. Hua, X. L. Lv, Z. Y. Huang, Y. Zou and C. L. Yang, *Adv. Mater.*, 2022, **34**, 2106954.
46 Y. Y. Qi, W. M. Ning, Y. Zou, X. S. Cao, S. L. Gong and C. L. Yang, *Adv. Funct. Mater.*, 2021, **31**, 2102017.
47 Y. X. Wang, K. Y. Di, Y. L. Duan, R. D. Guo, L. Y. Lian, W. Z. Zhang and L. Wang, *Chem. Eng. J.*, 2022, **431**, 133221.
48 Y. X. Wang, Y. L. Duan, R. D. Guo, S. F. Ye, K. Y. Di, W. Z. Zhang, S. Q. Zhuang and L. Wang, *Org. Electron.*, 2021, **97**, 106275.
49 M. L. Yang, S. Shikita, H. Min, I. S. Park, H. Shibata, N. Amanokura and T. Yasuda, *Angew. Chem., Int. Ed.*, 2021, **60**, 23142–23147.
50 M. L. Yang, I. S. Park and T. Yasuda, *J. Am. Chem. Soc.*, 2020, **142**, 19468–19472.
51 Y. Zhang, D. Zhang, J. Wei, Z. Liu, Y. Lu and L. Duan, *Angew. Chem., Int. Ed.*, 2019, **58**, 16912–16917.
52 Y. Xu, C. Li, Z. Li, J. Wang, J. Xue, Q. Wang, X. Cai and Y. Wang, *CCS Chem.*, 2022, **4**, 2065–2079.
53 Y. W. Zhang, D. D. Zhang, J. B. Wei, Z. Y. Liu, Y. Lu and L. Duan, *Angew. Chem., Int. Ed.*, 2019, **58**, 16912–16917.
54 F. Rauch, P. Endres, A. Friedrich, D. Sieh, M. Hahnel, I. Krummenacher, H. Braunschweig, M. Finze, L. Ji and T. B. Marder, *Chem. – Eur. J.*, 2020, **26**, 12951–12963.
55 Q. Y. Wang, Y. C. Xu, T. Yang, J. A. Xue and Y. Wang, *Adv. Mater.*, 2023, **35**, 2205166.
56 D. Karthik, D. H. Ahn, J. H. Ryu, H. Lee, J. H. Maeng, J. Y. Lee and J. H. Kwon, *J. Mater. Chem.*, 2020, **8**, 2272–2279.
57 Z. Y. Huang, H. H. Xie, J. S. Miao, Y. X. Wei, Y. Zou, T. Hua, X. S. Cao and C. L. Yang, *J. Am. Chem. Soc.*, 2023, **145**, 12550–12560.